energies

MDPI

Article

Conceptual Approach on Feasible Hydrogen Contents for Retrofit of CNG to HCNG under Heavy-Duty Spark Ignition Engine at Low-to-Middle Speed Ranges

Bum Youl Park [1], Ki-Hyung Lee [2] and Jungsoo Park [3,*]

[1] Department of Mechanical Design Engineering, Graduate School, Hanyang University, 1271 Sa 1-dong, Sangnok-gu, Ansan-si, Gyeonggi-do 426-791, Korea; pby9704@koreard.co.kr
[2] Department of Mechanical Design Engineering, Hanyang University, 1271 Sa 1-dong, Sangnok-gu, Ansan-si, Gyeonggi-do 426-791, Korea; kylee@hanyang.ac.kr
[3] Department of Mechanical Engineering, Chosun University, 309 Pilmun-daero, Dong-gu, Gwangju 61452, Korea
* Correspondence: j.park@chosun.ac.kr

Received: 10 June 2020; Accepted: 27 July 2020; Published: 28 July 2020

Abstract: Hydrogen-based engines are progressively becoming more important with the increasing utilization of hydrogen and layouts (e.g., onboard reforming systems) in internal combustion engines. To investigate the possibility of HICE (hydrogen fueled internal combustion engine), such as an engine with an onboard reforming system, which is introduced as recent technologies, various operating areas and parameters should be considered to obtain feasible hydrogen contents itself. In this study, a virtual hydrogen-added compressed natural gas (HCNG) model is built from a modified 11-L CNG (Compressed Natural Gas) engine, and a response surface model is derived through a parametric study via the Latin hypercube sampling method. Based on the results, performance and emission trends relative to hydrogen in the HCNG engine system are suggested. The operating conditions are 1000, 1300, and 1500 rpm under full load. For the Latin hypercube sampling method, the dominant variables include spark timing, excess air ratio (i.e., λ_{CH4+H2}), and H_2 addition. Under target operating conditions of 1000, 1300, and 1500 rpm, the addition of 6–10% hydrogen enables the virtual HCNG engine to reach similar levels of torque and BSFC (brake specific fuel consumption) compared to same lambda condition of λ_{CH4}. For the relatively low 1000 rpm speed under conditions similar to those of the base engine, NOx formation is greater than base engine condition, while a similar NOx level can be maintained under the middle speed range (1300 and 1500 rpm) despite hydrogen addition. Upon addition of 6–10% hydrogen under the middle speed operation range, the target engine achieves performance and emission similar to those of the base engine.

Keywords: HCNG; heavy-duty; Latin hypercube sampling; response surface model; virtual engine

1. Introduction

Sustainable and renewable energy sources are currently employed for powering mechanical systems. In particular, biogases are used as alternative fuels, either alone or blended with conventional fossil fuels or H_2 additives [1,2]. Hydrogen, as a combustion enhancer, can improve flame speed and range upon being added to fuels because of its favorable properties [3]. In this regard, many experimental and numerical studies yielding common results have been reported. It is widely known that as the hydrogen content of fuels increases, the in-cylinder pressure and temperatures also increase during combustion and thereby enhance engine torque [4,5]. However, as a result of such

elevated temperatures, the formation of NOx also increases, which is among the disadvantages of using hydrogen. Furthermore, many trials have been introduced with respect to the hydrogen content. Lather and Das studied comparison between CNG and HCNG engine performance and emission under sequential gas injection system. [3] By adding 10% and 18% of hydrogen in volume percent, the engine thermal efficiency and torque could be improved while NOx emission was increased. However, CO and CO_2 could be decreased remarkably. In recent review papers, higher percentages of hydrogen in CNG, more than 18% are not recommended, as lower methane number (MN) of the blend will result in a substantial drop in power. They implied that the possibility of engine knock cannot be ruled out for very high percentages of hydrogen in CNG, i.e., over 30% [6,7]. Research with 100% of hydrogen fueled engines was also introduced [4]. This study investigated the effect of varying the spark advance timing and excess air ratio (air excessive ratio: l) on the combustion and emission of nitrogen oxide (NOx) in a hydrogen-fueled spark ignition engine under part load conditions. Based on the results, it was concluded that the leanest mixture condition ($\lambda = 2.2$) with MBT spark timing exhibited the highest brake thermal efficiency of 34.17% and the NOx emissions were as low as 14 ppm.

There have also been many trials for HCNG fueled heavy-duty engines [8,9]. The idle performance of an 11-L, 6-cylinder engine equipped with a turbocharger and an intercooler was investigated under an idle speed of 600 rpm (Lee et al.) [8] The engine test results demonstrate that the use of HCNG enhanced idle combustion stability and extended the lean operational limit from excess air ratio 1.5 (CNG) to 1.6. A decrease of more than 25% in the fuel consumption rate was achieved in HCNG idle operations compared to CNG. Some NOx issues were carried out for the HCNG engines. To solve the NOx issues in HCNG, especially for heavy-duty engines, exhaust gas recirculation (EGR) has been implemented to lower the combustion temperatures. Park et al. introduced dilution strategies with EGR under stoichiometric and under lean burn conditions for 11 L heavy-duty engines, with 30% of H_2 content for 1250 rpm and 50% load. They found that the thermal efficiencies under stoichiometric combustion with EGR were lower than those under lean combustion, owing to a higher pumping loss and a lower combustion speed [8,9]. They implied that the hydrogen has an important role in lean burn limit extension under optimized excess air ratio and spark timing.

Given problems as well as the limitations pertaining to hydrogen production and storage, the concept of an onboard reforming system has become increasingly important, and the application of onboard reforming systems to engines is being actively investigated. Bogarra et al. studied catalytic onboard fuel reforming in gasoline direct-injection engines and derived benefits in terms of fuel economy and reductions in gaseous carbonaceous emissions and particulate matter [10]. Casanovas et al. conducted the catalytic reformation of pure ethanol and commercial bioethanol; they found that the hydrogen yield showed improvement similar to that achieved via onboard reforming [11]. Zhang et al. performed exhaust reformation in a natural gas (NG) engine under numerical and experimental conditions [12–15]. To examine the potential of natural gas engines in combination with a reformed exhaust gas recirculation (REGR) system, a zero-dimensional-based numerical study was performed to investigate the combustion characteristics of the reformer and NG homogenous charge compression ignition (HCCI) engine with exhaust-gas fuel reformation. It was observed that as the quantity of H_2 into the cylinder increased, the quantity of H atoms inside the cylinder also increased, which promoted H_2O_2 generation, as well as advanced and more intense engine combustion [12,13]. Moreover, it has been suggested that the REGR technique may be employed to achieve efficient and stable lean-burn combustion in marine engines fueled with natural gas [12,13]. The results indicate that the addition of hydrogen-rich reformate gases can extend the lean-burn limit. Furthermore, the combination of REGR and the lean-burn combustion strategy can improve the tradeoff relationship between NOx emissions and brake specific fuel consumption of NG-fueled marine engines [14,15]. With the objective of controlling emissions and mitigating performance loss in downsized spark-ignition engines, Catapan el al. suggested that exhaust gas recirculation (EGR) may be conducted to produce hydrogen gas via onboard catalytic steam reformation. Their results indicate the potential of producing an intake mixture with a 1% H_2 molar concentration at an engine speed

of 5000 rpm. Reduction in the engine speed, however, causes a reduction in H_2 because of the lower engine exhaust temperature. Although hot EGR presents a higher heat recovery potential, the heating value of the fuel is substantially decreased owing to the recirculation of inert gases [16].

Recent research investigations have also shown that mounting an onboard reforming system to an internal combustion engine has many effects. However, existing engine systems are becoming more complex in terms of subsystem application, considering hydrogen supply and application. Various tendencies can therefore be observed under each operating condition of the engine system. Through system-level analysis, several means for including a wide range of engine parameters are found to be available.

In addition, the connecting research between existing HCNG-based research and HCNG characteristics by onboard reforming is important. From this point of view, it is necessary to analyze from the system to component by proposing a proper range of hydrogen content by onboard reforming. This study is the first step for this approach. The purpose of this study is to suggest the proper range of hydrogen that has been applied to HCNG in various ways to the range of hydrogen content when applying onboard reforming. In addition, the method to maintain the performance and emission level of the base CNG engine was observed under retrofitter HCNG from the system point of view. To achieve the research goal, engine system analysis including crank train was numerically performed. A virtual hydrogen-added compressed natural gas (HCNG) model was built from a modified 11-L CNG engine, and a response surface model was derived through a parametric study based on the Latin hypercube sampling method. Accordingly, identification of the performance and emission trends in the HCNG engine system relative to hydrogen is suggested without an onboard fuel reforming system. In the future work, hydrogen contents suggested by the present study will be achieved, including detailed combustion analysis that considers fuel reforming reaction.

2. Model Description

2.1. Target Engine and Detailed One-Dimensional Engine Modeling

The target engine of this study is a large 11-L natural gas engine. The specifications of this base engine are summarized in Table 1.

Table 1. Engine specifications and operating conditions.

Item	Specification
Engine type	In-line 6
Bore	123 mm
Stroke	155 mm
Displacement	11 L
Compression ratio	13:1
Intake system	Waste-gate Turbocharger
Max. power	250 kW@2100 rpm
Max. torque	140 kgm@1300 rpm
Speed	1000, 1300, 1500 rpm
Load	Full load

These specifications as well as the experimental results of each component of the target engine are provided by an engine development company according to engine dynamometer test. Based on the engine specifications and test results obtained from OEM (Original Equipment Manufacturer), the base engine model was constructed. Detailed test conditions are shown in Table 2.

Table 2. Engine test conditions offered by OEM (Original Equipment Manufacturer).

Test Conditions at Each rpm	1000 rpm	1300 rpm	1500 rpm
Load (%)	100	100	100
BMEP (bar)	13.9	15.4	15.1
Boost pressure (bar)	1.92	2.29	2.27
Excess air ratio, lambda (-)	1.54	1.56	1.56

A numerical analysis is conducted using GT-POWER, which is software designed for engine cycle simulations based on thermodynamics; a more detailed explanation can be found in our previous study [17].

To build a fast running model, the turbocharger only simulates the rear and front ends of the compressor and turbine, respectively. The inputted boundary conditions are based on a look-up table of boost pressure, temperature, and turbine shear pressure and temperature.

The combustion process is analyzed using a two-zone model employed in our previous numerical analysis of a gas engine generator fueled with CH_4–H_2 blends [17]. For every time step in each zone, energy, mass, and momentum conservation equations are solved separately [17,18]. The primary equations used for describing the combustion behavior to indicate mass entrainment in the flame front, burn rate, and flame speed are as follows:

$$\frac{dM_e}{dt} = \rho_e A_e (S_T + S_L) \tag{1}$$

$$\frac{dM_b}{dt} = \frac{(M_e - M_b)}{\tau} \tag{2}$$

where M_e /dt and M_b /dt are the entrainment rate for the unburned and burned mass, A_e is the flame front area, S_T and S_L are the turbulent and laminar flame speeds.

For CH_4 with hydrogen content, S_L in Equation (1) has to be specified by considering hydrogen content. In the present study, therefore, the laminar flame speeds considered for CH_4 and hydrogen mixed with air are based on our previous research [19,20], and NO_X formation calculations are based on the extended Zeldovich mechanism, which is well known as thermal NO_X formation processes depending on temperature [21].

To describe combustion conditions with respect to the air–fuel relationships, two types of excess air ratio are used for this study, λ_{CH4} and λ_{CH4+H2}. λ_{CH4}, the methane basis excess air ratio, and $\lambda_{CH4+H2.}$, the hydrogen added methane basis excess air ratio, are expressed as follows:

$$\lambda_{CH_4} = \frac{\left(\dot{m}_{air} / \dot{m}_{CH_4}\right)_{actual}}{\left(\dot{m}_{air} / \dot{m}_{CH_4}\right)_{stoichiometric}} \tag{3}$$

$$\lambda_{CH_4+H_2} = \frac{\left(\dot{m}_{air} / \dot{m}_{CH_4+H_2}\right)_{actual}}{\left(\dot{m}_{air} / \dot{m}_{CH_4+H_2}\right)_{stoichiometric}} \tag{4}$$

Since the lambda control used in the actual target engine is a hydrocarbon fuel control method using an oxygen sensor, there may be a limitation in reflecting the lambda according to the hydrogen content. Therefore, in this study, total lambda containing hydrogen was used as an index that contains hydrogen content.

Please note that lambda for the base engine fueled with CNG uses Equation (3), while a virtual HCNG engine introduced in this study uses Equation (4).

Hydrogen content can be written as follow:

$$H_2\ Percentage\ in\ volume\ (\%\ \text{vol.}) = \frac{Volume\ fraction\ of\ hydrogen\ in\ total\ fuel}{Volume\ fraction\ of\ total\ fuel} \times 100\% \quad (5)$$

2.2. Latin Hypercube Sampling for the Response Surface Model

The Latin hypercube sampling (LHS) method, which is a type of fractional experiment design, is employed to comprehend engine performance and emission trends according to the independent variables of the virtual engine model. The LHS method is a technique first described by McKay et al. [22]. In the statistical sampling area, a square grid (including sample positions) is called Latin square with a hyperplane if, and only if, there is one sample in each row and each column [23]. The Latin hypercube has a desired sampling number whereby each sample is the only sample in every axis-aligned hyperplane in which it is included [22]. Compared to the full factorial design of experiment (DoE), the advantages of the LHS method are to provide relatively faster optimization processes by considering many independent variables with fewer sampling points.

In this study, 150 sampling points at each engine speed-rpm full-load condition are used at different spark timings, total excess air ratios (i.e., λ_{CH4+H2}), and H_2 fractions. When H_2 is added to the CNG engine system, basic excess air ratio λ_{CH4} must be recalculated and the optimum spark timing range is changed, owing to hydrogen's fast flame speed and wide flammable ranges. Therefore, hydrogen content, spark timing and excess air ratio including hydrogen content have to be considered together.

The selected variable ranges for the LHS are summarized in Table 3.

Table 3. Sampling ranges for each variables and the number of sampling points.

Variables	Sampling Ranges	# of Sampling Points
Spark timing (CA aTDC)	from −50 to −10	150 sampling pointsat each speed condition
Total excess air ratio	1.2–2.0	
Hydrogen content (vol. %)	5–15	

Here, the LHS is very effective in developing the first- and second-order responses for regression model development with minimal numerical or experimental data sampling points. Based on the LHS method, regression analysis employing the radial basis function is performed to generate the response surface. Figure 1 shows the overall process for the present research. More detailed explanations for DoE and LHS for engine analysis are thoroughly described in our previous work [17,19,23,24].

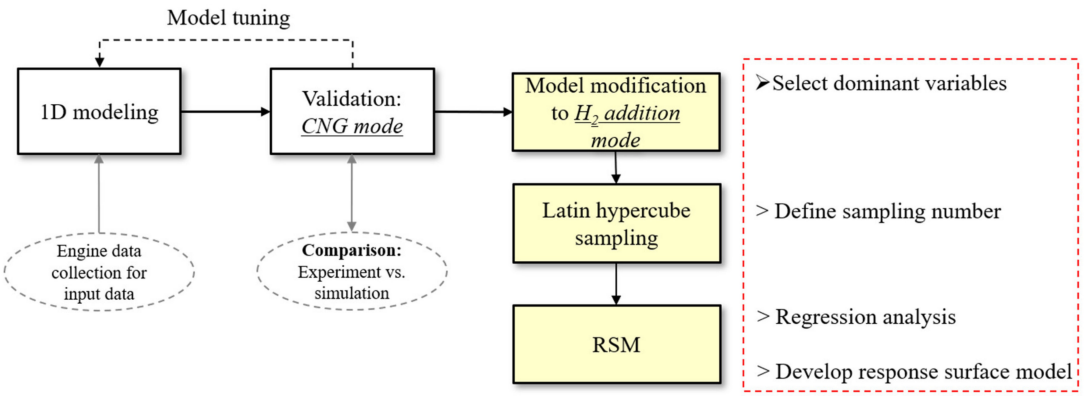

Figure 1. Overall research flow.

3. Results and Discussions

3.1. Validation Results and Response Surface from Latin Hypercube Sampling

Figure 2 compares the test and analysis results of the base engine; Figure 3 shows the model validation results. The validation indicates that the numerical model of the base CNG engine conforms well to thermodynamic properties, performances, and emissions, within 5% on an average. In an engine model, detailed turbocharging motion was not included because the turbocharger only simulates the rear and front ends of the compressor and turbine to build a fast running model. This simplified modeling method can cause some errors between simulation and test results. Nevertheless, model accuracy usually seems acceptable.

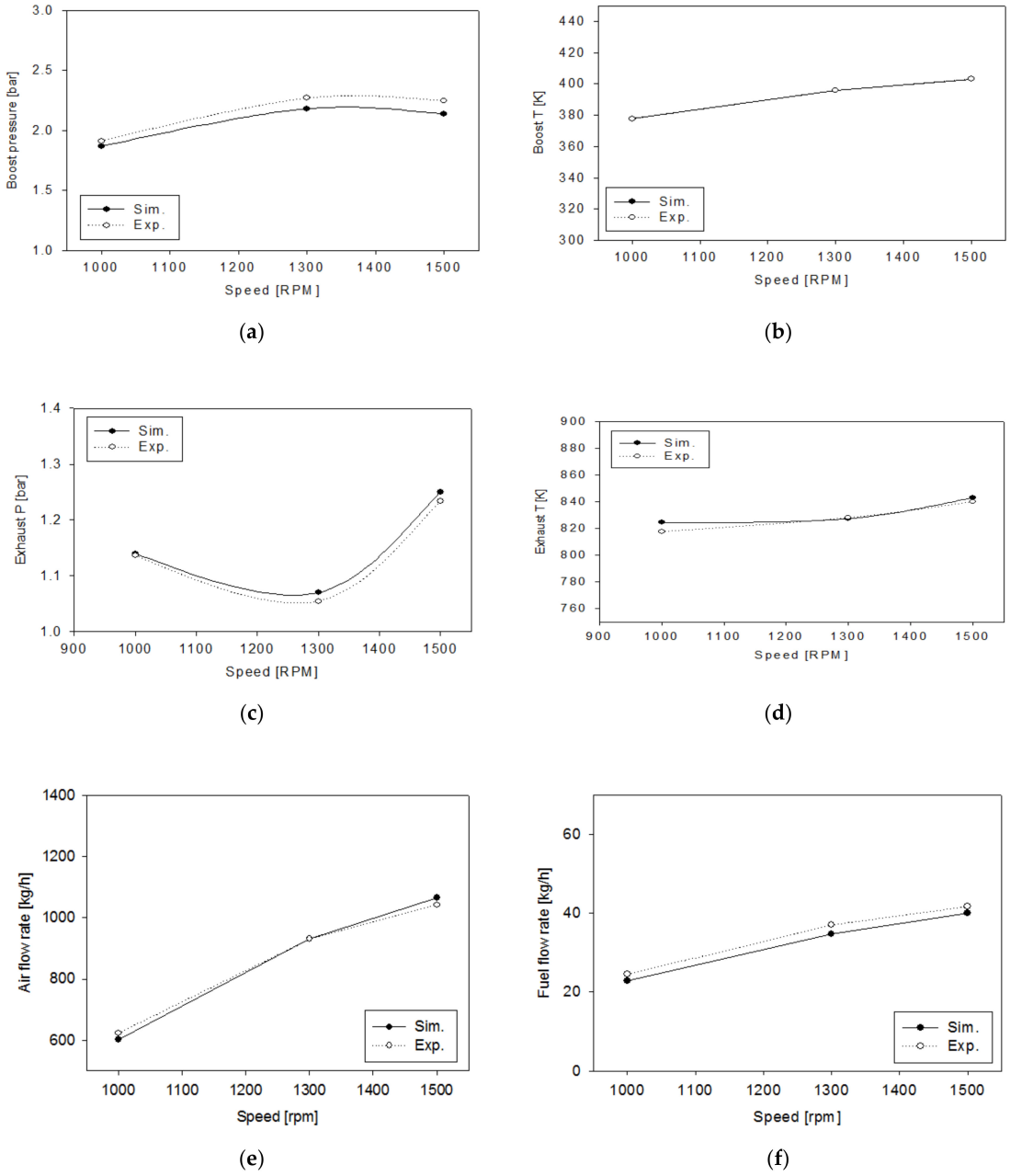

Figure 2. Validation results for thermodynamic and fluidic properties at engine components: (**a**) boost pressure@upstream of intercooler; (**b**) boost temperature@upstream of intercooler; (**c**) exhaust pressure@upstream of turbine; (**d**) exhaust temperature@upstream of turbine; (**e**) air flow rate; (**f**) fuel flow rate.

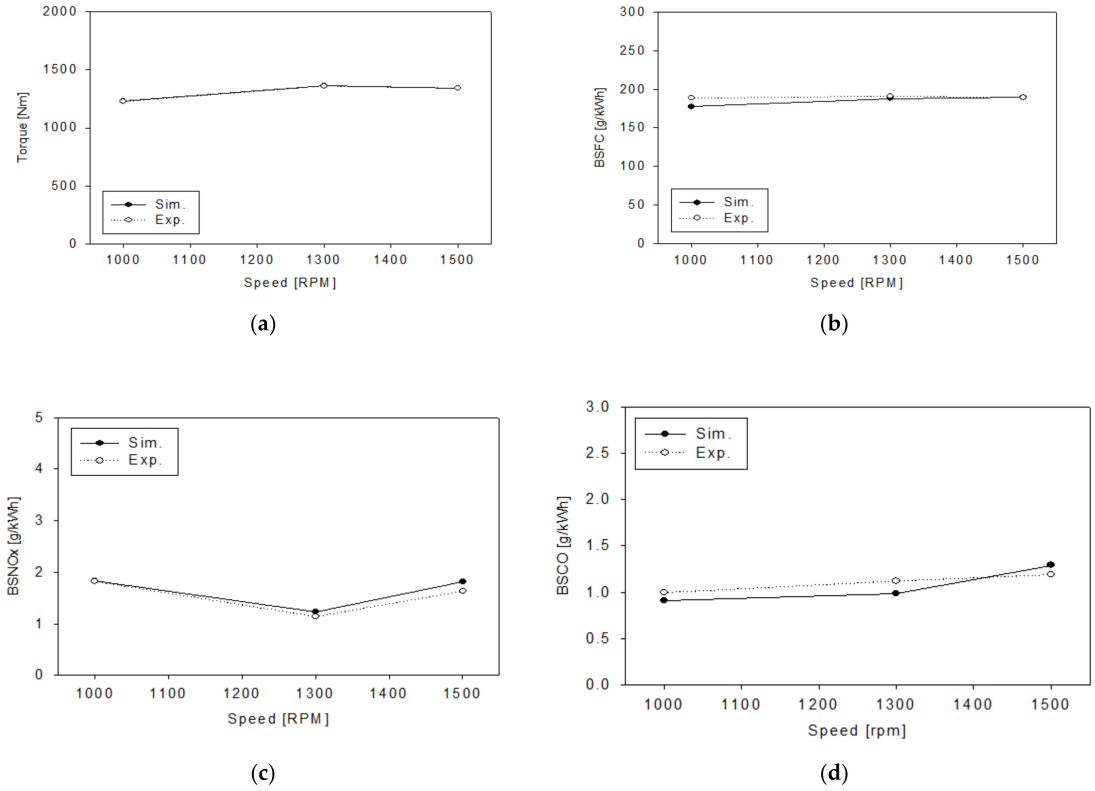

Figure 3. Validation results for engine performance and emission: (**a**) brake torque; (**b**); BSFC; (**c**) BSNOx; (**d**) BSCO.

Detailed errors and standard errors for validation results are shown in Tables 4 and 5 at each rpm. Based on the validation results, it is shown that the model could well predict thermodynamic and fluid dynamic properties. However, the 1D engine model has weaknesses in prediction of combustion products even if the predictive combustion model was used. These kinds of issues can be solved by coupling with 3D combustion analysis and will be performed in future work. This study focuses on the performance and emission tendencies from a systematic point of view.

Table 4. Detailed errors and standard errors for validation results for data shown in Figure 2.

RPM	*Boost P*	*Boost T*	*Exhaust P*	*Exhaust T*	*Air Flow Rate*	*Fuel Flow Rate*
Error, % @1000	−2.28	−0.18	0.32	0.84	−3.37	−4.17
Error, % @1300	−3.87	−0.22	1.45	−0.10	0.21	−5.41
Error, % @1500	−4.90	−0.25	1.29	0.35	2.19	−4.76
Standard error (%) Abs. value	3.68	0.22	1.02	0.43	1.92	4.78

Table 5. Detailed errors and standard errors for validation results for data shown in Figure 3.

RPM	**Torque**	**BSFC**	**BSNOx**	**BSCO**
Error, % @1000	0.28	−5.90	0.55	−7.52
Error, % @1300	0.08	−1.61	5.26	−2.03
Error, % @1500	−0.06	0.40	4.69	6.78
Standard error (%) Abs. value	0.14	2.64	3.50	5.44

Figure 4 shows the tendency of the total lambda when considering the methane-based lambda and hydrogen content. This is based on the sampling point and hydrogen fraction of independent variables employed for implementing the LHS-based DoE. Herein, the methane-based lambda is the

lambda value when the hydrogen content is neglected despite the addition of this gas, whereas the total lambda is the lambda value converted when considering the hydrogen content. A linear shape can be observed when the total lambda is converted according to the methane-based lambda. Since the lambda control used in the actual target engine is a hydrocarbon fuel control method using an oxygen sensor, there may be a limitation in reflecting the lambda according to the hydrogen content. Therefore, in this study, total lambda containing hydrogen was used as an index that contains hydrogen content.

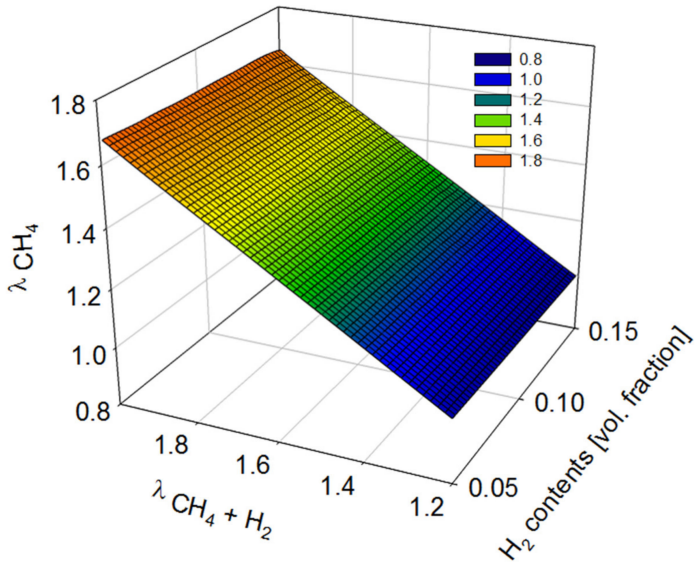

Figure 4. Relationship between total excess air ratio and excess air ratio of CH_4 when considering hydrogen content.

3.2. Response Surface Model under a 1000 rpm Full-Load Condition

Figures 5–7 show the response surface model (RSM) derived at a 1000 rpm full load in terms of brake torque, brake specific fuel consumption (BSFC), and brake specific NOx (BSNOx), respectively. The brake torque results obtained under a 1000 rpm full-load condition derived from the LHS-based DOE are shown in Figure 5.

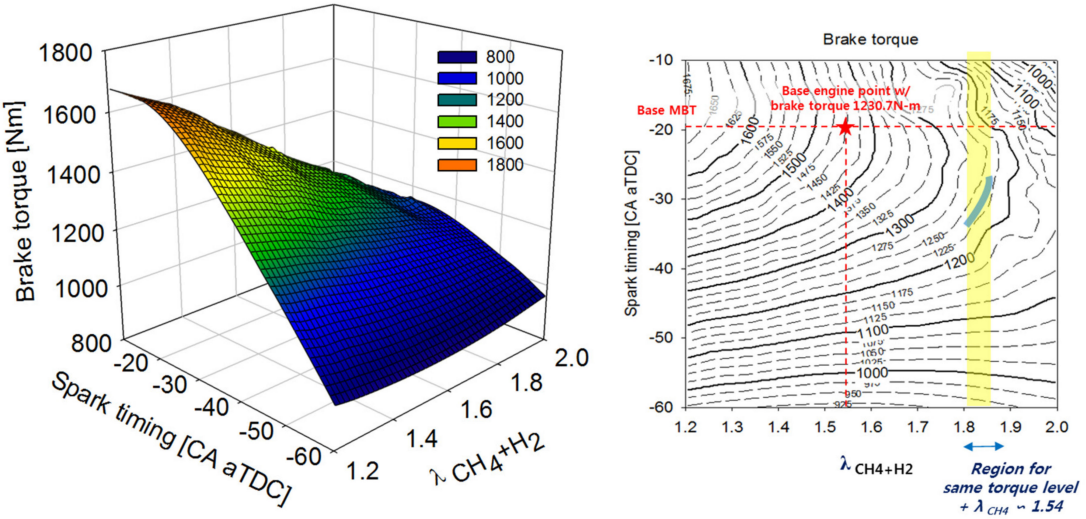

Figure 5. Response surface model: brake torque as functions of spark timing and hydrogen added methane based EAR @1000 rpm.

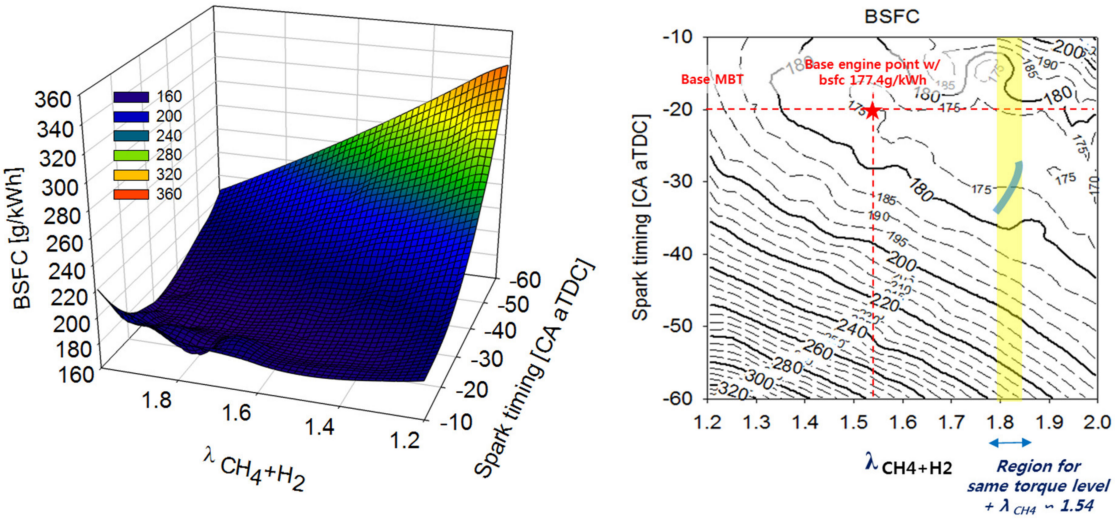

Figure 6. Response surface model: brake specific fuel consumption as functions of spark timing and hydrogen added methane based EAR @1000 rpm.

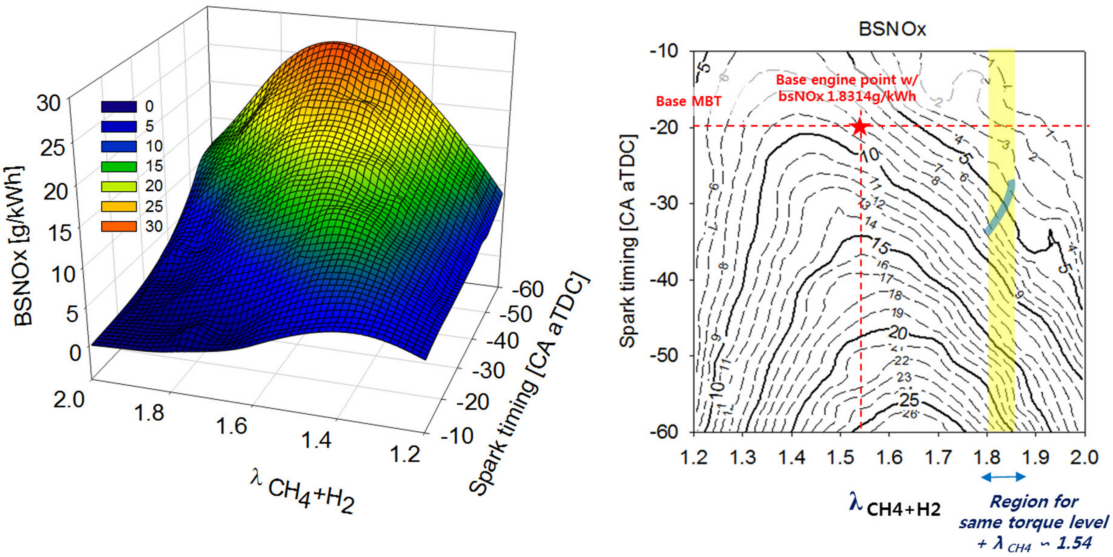

Figure 7. Response surface model: brake specific NOx as functions of spark timing and hydrogen added methane based EAR @1000 rpm.

As a result of hydrogen addition, a −50 aTDC or higher spark timing shows that the torque reaches the maximum brake torque (MBT) and thereafter decreases. Moreover, to achieve the same torque (1230.7 N·m) as that of the base engine, hydrogen is added, resulting in a considerably higher MBT; the same torque is implemented in regions other than the MBT point (blue line in the figure). The possibility of increasing torque via hydrogen addition is thereby demonstrated. From Figure 4, it can be observed that when the total lambda remains equal to the base engine lambda of 1.54 as shown in Table 2, that is, the MBT advances between 1.8 and 1.85 of the total lambda, the same level of torque as that of the base engine is achieved. This therefore suggests that the same torque may be realized in the region where the lean flammability limit is extended upon hydrogen addition.

Figure 6 shows the results of BSFC under the 1000 rpm full-load condition derived from the LHS-based DOE. When compared with the brake torque, the BSFC rate exhibits a reverse contour shape and is found to be considerably related to torque. In the two-dimensional contour graph expression, it is observed that fuel efficiency tends to increase as the hydrogen content increases. The foregoing is a mass substitution effect that occurs when hydrogen occupies the methane fraction of the main

fuel. Nevertheless, it is further observed that brake specific fuel consumption can be improved even with the addition of a small amount of hydrogen because this gas possesses a large volumetric lower heating value. Moreover, advanced spark timing under hydrogen addition can cause higher power output. Moreover, for the same torque level (blue line in figure) as that of the base engine, this degree of fuel efficiency can be realized as the MBT advances with hydrogenation and by controlling the spark timing, indicating the possibility of achieving a better fuel consumption rate. Based on Figure 4, if the total lambda remains equal to the base engine lambda of 1.54, that is, the MBT is between 1.8 and 1.85 of the total lambda, then this will be sufficient to achieve the same level of BSFC as that of the base engine.

Figure 7 shows the BSNOx results obtained under a 1000 rpm full load derived from the LHS-based DOE. Compared with the BSNOx of brake torque and BSFC, the nitrogen oxide emissions at the same base engine torque level (blue line) further increases with hydrogen addition. This is because as the combustion temperature increases with the addition of hydrogen, the thermal NOx formation increases, as has been widely confirmed by existing experimental results.

The analysis indicates that when the HCNG heavy-duty engine runs at 1000 rpm, a distinct tradeoff between torque or fuel economy and NOx emission exists; nevertheless, on considering the torque loss when lean combustion is achieved by increasing the hydrogen fraction, the foregoing suggests that BSNOx formation can be reduced.

3.3. Response Surface Model under a 1300 rpm Full-Load Condition

Figures 8–10 show the RSM derived at 1300 rpm full load in terms of brake torque, BSFC, and BSNOx, respectively. Figure 8 shows the results of brake torque under a 1300 rpm full-load condition derived from the LHS-based DOE. The figure indicates that with the addition of hydrogen, the MBT is attained, and the torque decreases thereafter over the entire area of the variable spark sweep timing. Moreover, to achieve the same torque (1350 N·m) as that of the base engine, a more advanced MBT appears upon hydrogen addition; it is also possible to implement the same torque (blue line in figure) as that of the base engine in an advanced state in areas other than the MBT point. According to Figure 4, when the total lambda remains equal to the base engine lambda of 1.56 as shown in Table 2, that is, if the MBT advances between 1.85 and 1.9 of the methane-based lambda, the same torque as that of the base engine can be achieved.

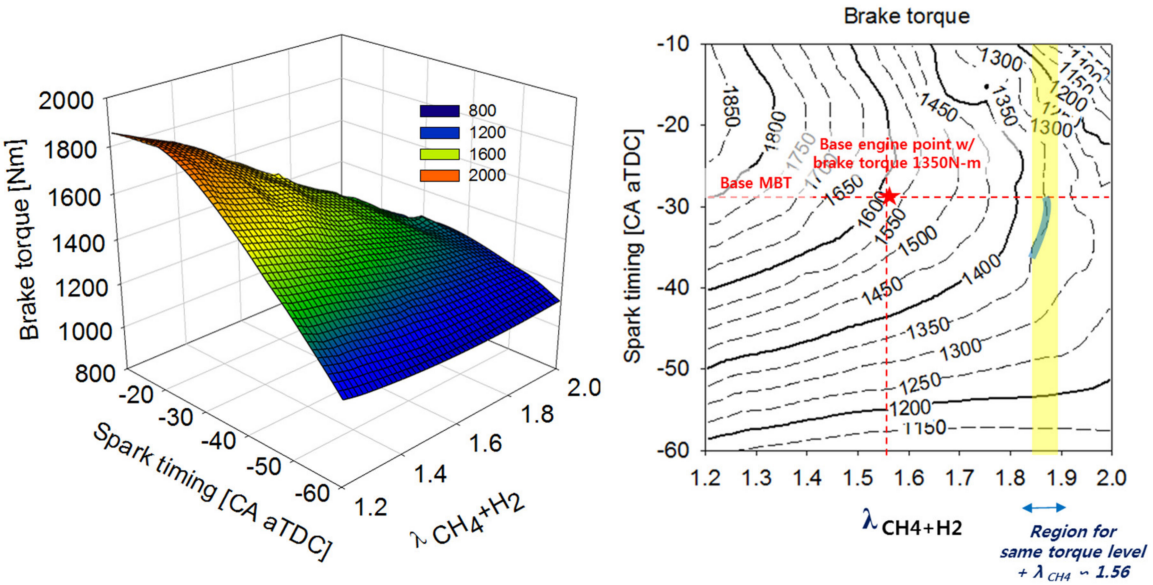

Figure 8. Response surface model: brake torque as functions of spark timing and hydrogen added methane based EAR @1300 rpm.

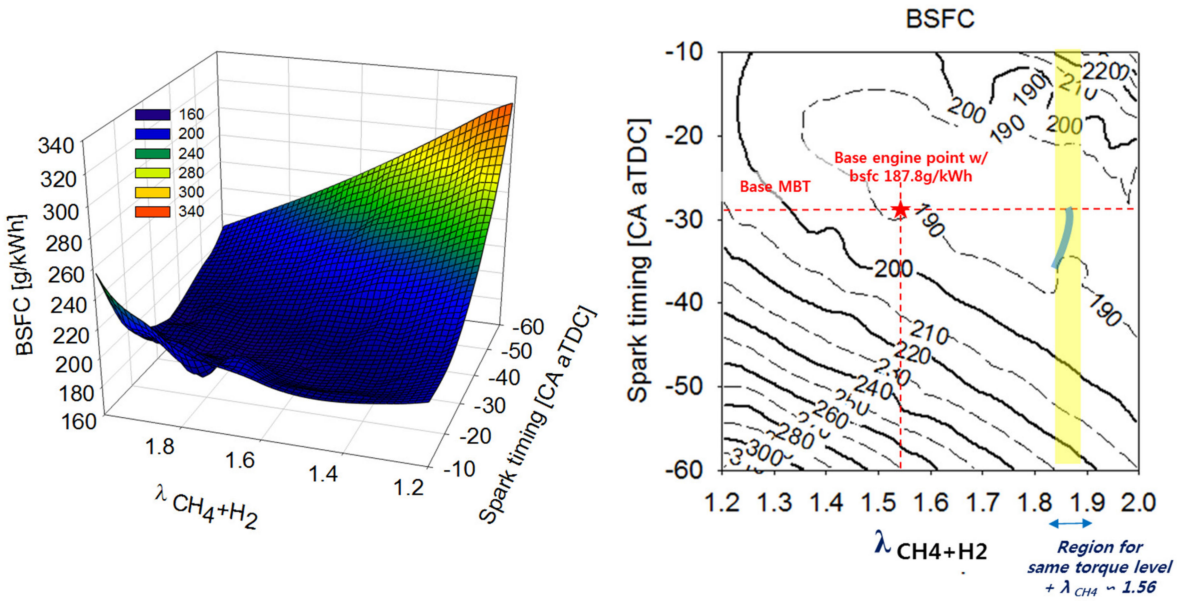

Figure 9. Response surface model: brake specific fuel consumption as functions of spark timing and hydrogen added methane based EAR @1300 rpm.

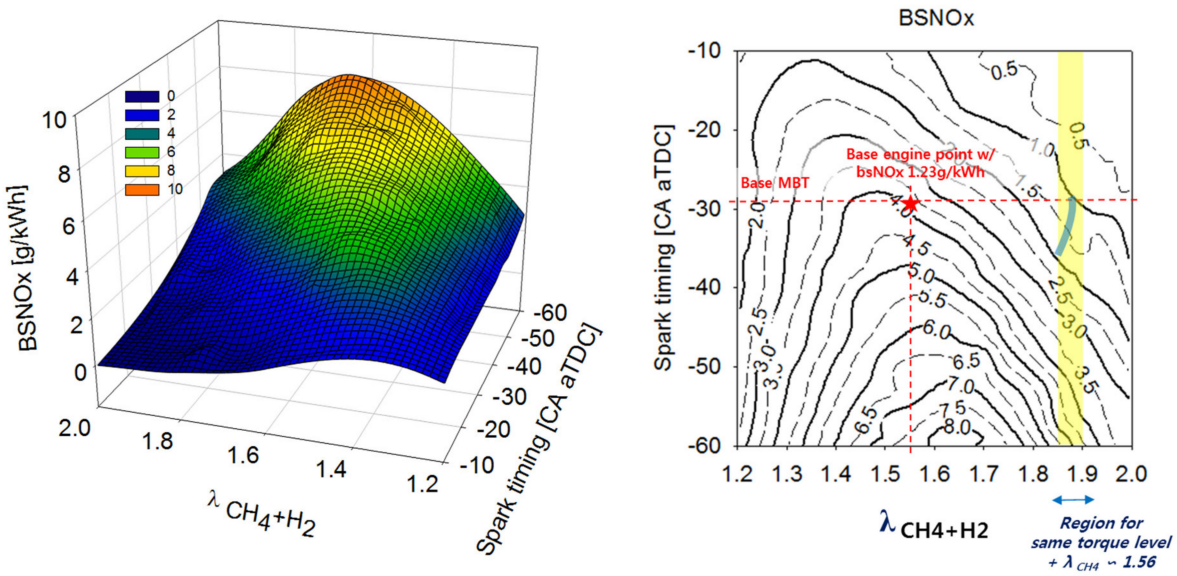

Figure 10. Response surface model: brake specific NOx as functions of spark timing and hydrogen added methane based EAR @1300 rpm.

Figure 9 shows the results of BSFC under a 1300 rpm full-load condition derived from the LHS-based DOE. When compared with the brake torque, the BSFC rate exhibits a reverse contour shape and is observed to be considerably related to the torque. When expressed in the form of a two-dimensional contour graph, the fuel efficiency tends to increase as hydrogen addition increases, which is a mass substitution effect that occurs when hydrogen occupies the methane fraction of the main fuel. It is further observed that brake specific fuel consumption can be improved even with the addition of a small amount of hydrogen because this gas possesses a large volumetric lower heating value. Moreover, advanced spark timing under hydrogen addition can cause higher power output. To achieve the same torque level (blue line in figure) as that of the base engine, a similar fuel efficiency can be realized regarding the more advanced MBT via hydrogenation and by controlling the spark timing in the vicinity of the MBT as hydrogen is added; this indicates the possibility of achieving a better fuel consumption rate. Based on Figure 4, when the total lambda remains equal to 1.56 of the

base engine lambda, that is, if the MBT condition is between 1.85 and 1.9 of the total lambda, then the same level of BSFC as that of the base engine can be achieved.

Figure 10 shows the BSNOx results obtained under the 1300 rpm full-load condition derived from the LHS-based DOE. In this case, nitrogen oxide formation at the same torque level (blue line in the figure) as that of the base engine can be maintained through hydrogen addition.

Upon introduction of hydrogen to the heavy-duty HCNG engine, it is possible to achieve fuel economy and maintain a similar level of BSNOx emission at 1300 rpm without the loss of torque.

3.4. Response Surface Model under a 1500 rpm Full-Load Condition

Figures 11–13 show the RSM derived at a 1500 rpm full load in terms of brake torque, BSFC, and BSNOx, respectively. Figure 11 shows the results of brake torque obtained under a 1500 rpm full-load condition derived from the LHS-based DOE. It shows that as hydrogen is added, the torque increases and attains the MBT value; thereafter, it decreases over the entire area of variable spark sweep timing. Furthermore, to achieve the same torque (1342 N·m), a more advanced MBT is observed when hydrogen is added. The same torque as that of the base engine is realized in the advanced and perceived states, even in areas other than the MBT point (blue line in the figure). Based on Figure 4, when the total lambda remains equal to the base engine lambda of 1.56 as shown in Table 2, that is, if the advanced and perceived MBT condition is between 1.85 and 1.9 of the total lambda, then the same level of torque as that of the base engine can be achieved.

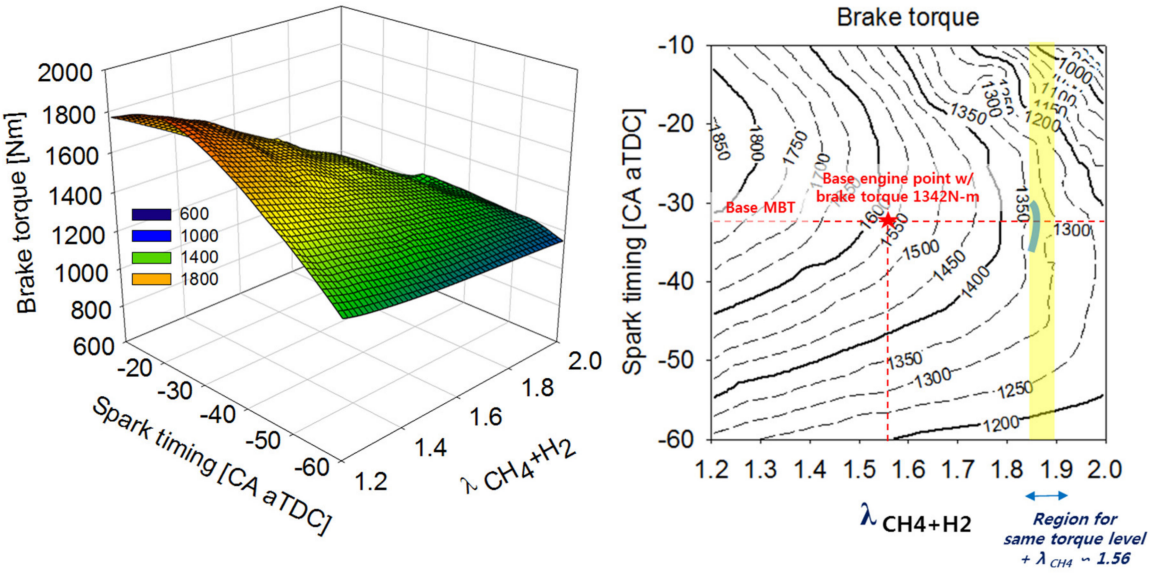

Figure 11. Response surface model: brake torque as functions of spark timing and hydrogen added methane based EAR @1500 rpm.

Figure 12 shows the results of BSFC under a 1500 rpm full-load condition derived from the LHS-based DOE. When compared with the brake torque, the BSFC rate exhibits a reverse contour shape and is found to be considerably related to the torque. In the two-dimensional contour graph expression, it is observed that fuel efficiency tends to increase as the amount of hydrogen added increases. This is a mass substitution effect that occurs when hydrogen occupies the methane fraction of the main fuel. It is further observed that brake specific fuel consumption can be improved even with the addition of a small amount of hydrogen because this gas possesses a large volumetric lower heating value. Moreover, advanced spark timing under hydrogen addition can cause higher power output. With the same torque level (blue line in the figure) as that of the base engine, a similar fuel efficiency can be realized through hydrogenation to advance the MBT, spark timing, and perceptual control near the MBT, indicating the potential for achieving a better fuel consumption rate. Based on Figure 4, if the

total lambda remains equal to the base engine lambda of 1.56, that is, if the MBT condition is between 1.85 and 1.9 of the total lambda, then the same level of BSFC as that of the base engine can be achieved.

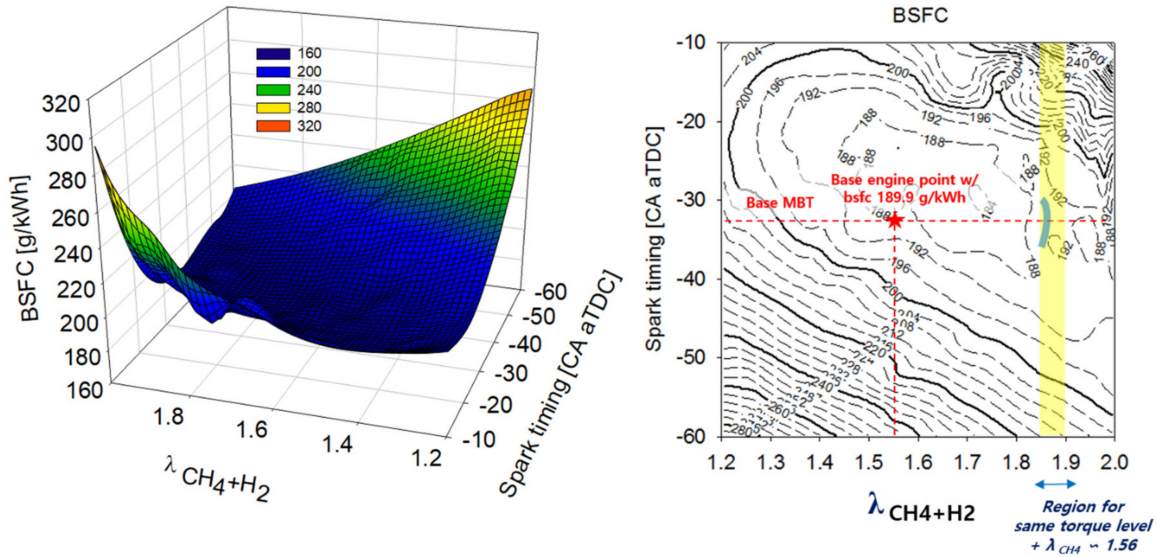

Figure 12. Response surface model: brake specific fuel consumption as functions of spark timing and hydrogen added methane based EAR @1500 rpm.

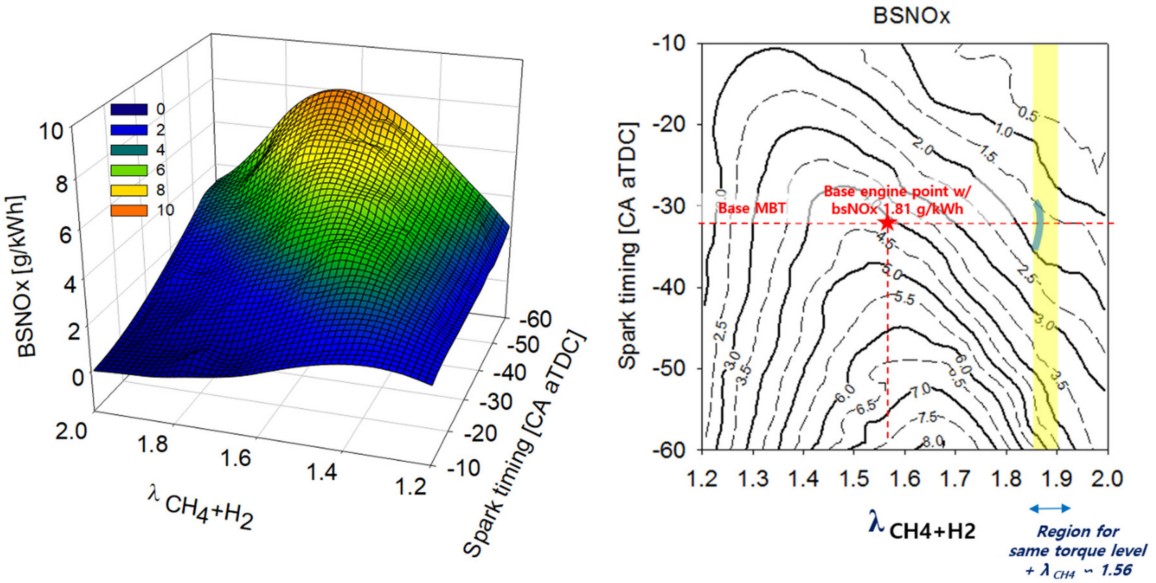

Figure 13. Response surface model: brake specific NOx as functions of spark timing and hydrogen added methane based EAR @1500 rpm.

Figure 13 shows the BSNOx results obtained under a 1500 rpm full load derived from the LHS-based DOE. In this case, nitrogen oxide formation at the same torque level (blue line in the figure) as that of the base engine can be maintained through hydrogen addition.

With the addition of hydrogen to the heavy-duty HCNG engine, it is possible to achieve fuel economy and a similar or lower level of BSNOx emission at 1500 rpm without loss of torque; this result is similar to that achieved at an engine speed of 1300 rpm.

4. Conclusions

The fundamental characteristics of a large 11-L heavy duty HCNG engine are investigated using a one dimensional cycle simulation and the LHS method. The numerical results of this study can be summarized as follows:

- Based on experimental data, a 1D gas engine generator is modeled and validated. The LHS method is employed to obtain the RSM as a fractional factorial DOE considering random sampling, spark timing, excess air ratio, and H_2 content, as independent variables within the desired ranges.
- Using fuel containing 6–10% hydrogen under all target operating conditions, the virtual HCNG engine is observed to be capable of reaching similar levels of torque and BSFC for the same lambda (i.e., $\lambda_{CH_4+H_2}$). Moreover, NOx formation loss is observed in the region where engine speed is relatively low (i.e., 1000 rpm) under conditions similar to those of the base engine. On the contrary, NOx loss can be avoided despite hydrogen addition in the relatively middle speed region (1300 and 1500 rpm). With fuel containing 6–10% hydrogen, it is possible to achieve performance and emission similar to those of the base engine in the middle speed operation range of the large engine. This demonstrates the application potential of hydrogen addition by considering achievable hydrogen yield from onboard reforming system.
- The results suggest that the yields of onboard reforming as reported by many studies are suitable for the middle speed ranges of heavy-duty HCNG engine operation in terms of performance and emissions. In future work, the characteristics of the HCNG engine under high speed ranges will also be taken into consideration relative to CO emissions, and the hydrogen content map for all operating speeds will be suggested for COx-free engine systems. Based on the performance and emission tendencies conducted from the present work, system to component analysis will be taken under feasible hydrogen contents. By connecting to 3D combustion analysis, detailed engine concepts will be conducted and reformer concepts will be introduced to achieve hydrogen yield suggested in this study.

Author Contributions: Conceptualization, investigation, methodology, B.Y.P. and J.P.; formal analysis, B.Y.P.; writing—original draft preparation, B.Y.P.; writing—review and editing, K.-H.L. and J.P.; supervision, K.-H.L. and J.P.; project administration, B.Y.P. and J.P. All authors have read and agreed to the published version of the manuscript.

Funding: This work was funded by the Ministry of Trade, Industry, and Energy (MoTIE, Korea).

Acknowledgments: This work was supported by the Technology Innovation Program (No. 20005881; Development of technology for power generation system with advanced combustion engine for range-extended electric vehicle (REEV) with power output greater than 15 kW and fuel efficiency smaller than 270 g/kWh) funded by the Ministry of Trade, Industry, and Energy (MoTIE, Korea).

Conflicts of Interest: The authors declare no conflict of interest.

Abbreviations

aTDC	After top dead center
BSNOx	Brake specific nitrogen oxides
BSCO	Brake specific carbon monoxide
CA	Crank angle
CO	Carbon monoxide
CR	Compression ratio
DoE	Design of experiment
EAR	Excess air ratio
HCNG	Hydrogen-added compressed natural gas
LHS	Latin hypercube sampling
NO_x	Nitric oxides
RSM	Response surface model
SI	Spark ignition

Nomenclature

m_u unburned zone mass, kg
m_b burned zone mass, kg
m_f fuel mass, kg
m_a air mass, kg
h_f fuel mass enthalpy, J/kg
h_a air mass enthalpy, J/kg
$h_{f,i}$ injected fuel mass enthalpy, J/kg
e_u unburned zone energy, kW
e_b burned zone energy, kW
p cylinder pressure, bar
V_u unburned zone volume, m^3
V_b burned zone volume, m^3
Q_u unburned zone heat transfer, kW
Q_b burned zone heat transfer, kW
λ excess air ratio

References

1. Yan, F.; Xu, L.; Wang, Y. Application of hydrogen enriched natural gas in spark ignition IC engines: From fundamental fuel properties to engine performances and emissions. *Renew. Sustain. Energy Rev.* **2018**, *82*, 1457–1488. [CrossRef]
2. Dhyani, V.; Subramanian, K.A. Experimental based comparative exergy analysis of a multi-cylinder spark ignition engine fuelled with different gaseous (CNG, HCNG, and hydrogen) fuels. *Int. J. Hydrog. Energy* **2019**, *44*, 20440–20451. [CrossRef]
3. Lather, R.S.; Das, L.M. Performance and emission assessment of a multi- cylinder SI engine using CNG & HCNG as fuels. *Int. J. Hydrog. Energy* **2019**, *44*, 21181–21192.
4. Alrazen, H.A.; Ahmad, K.A. HCNG fueled spark-ignition (SI) engine with its effects on performance and emissions. *Renew. Sustain. Energy Rev.* **2018**, *82*, 324–342. [CrossRef]
5. Zhao, J.; Ma, F.; Xiong, X.; Deng, J.; Wang, L.; Naeve, N.; Zhao, S. Effects of compression ratio on the combustion and emission of a hydrogen enriched natural gas engine under different excess air ratio. *Energy* **2013**, *59*, 635–658. [CrossRef]
6. Mehra, R.K.; Duan, H.; Juknelevicius, R.; Ma, F.; Li, J. Progress in hydrogen enriched compressed natural gas (HCNG) internal combustion engines e a comprehensive review. *Renew. Sustain. Energy Rev.* **2017**, *80*, 1458–1498. [CrossRef]
7. Lee, J.; Park, C.; Bae, J.; Kim, Y.; Choi, Y.; Lim, B. Effect of different excess air ratio values and spark advance timing on combustion and emission characteristics of hydrogen-fueled spark ignition engine. *Int. J. Hydrog. Energy* **2019**, *44*, 25021–25030. [CrossRef]
8. Lee, S.; Kim, C.; Choi, Y.; Lim, G.; Park, C. Emissions and fuel consumption characteristics of an HCNG-fueled heavy-duty engine at idle. *Int. J. Hydrog. Energy* **2014**, *39*, 8078–8086. [CrossRef]
9. Park, C.; Lee, S.; Kim, C.; Choi, Y. A comparative study of lean burn and exhaust gas recirculation in an HCNG-fueled heavy-duty engine. *Int. J. Hydrog. Energy* **2017**, *42*, 26094–26101. [CrossRef]
10. Bogarra, M.; Herreros, J.M.; Tsolakis, A.; York, A.P.E.; Millington, P.J. Study of particulate matter and gaseous emissions in gasoline direct injection engine using on-board exhaust gas fuel reforming. *Appl. Energy* **2016**, *180*, 245–255. [CrossRef]
11. Casanovas, A.; Divins, N.; Rejas, A.; Bosch, R.; Llorca, J. Finding a suitable catalyst for on-board ethanol reforming using exhaust heat from an internal combustion engine. *Int. J. Hydrog. Energy* **2016**, *42*, 13621–13690. [CrossRef]
12. Zhang, Z.; Jia, P.; Reng, S.; Liang, J.; Long, Y.; Li, G. Numerical simulation of exhaust reforming characteristics in catalytic fixed-bed reactors for a natural gas engine. *Chem. Eng. Sci.* **2018**, *191*, 200–207. [CrossRef]
13. Zhang, Z.; Xie, Q.; Liang, J.; Li, G. Numerical study of combustion characteristics of a natural gas HCCI engine with closed loop exhaust-gas fuel reforming. *Appl. Therm. Eng.* **2017**, *119*, 430–437. [CrossRef]

14. Li, G.; Long, Y.; Zhang, Z.; Liang, J.; Zhang, X.; Zhang, X.; Wang, Z. Performance and emissions characteristics of a lean-burn marine natural gas engine with the addition of hydrogen-rich reformate. *Int. J. Hydrog. Energy* **2019**, *44*, 31554–31556. [CrossRef]
15. Long, Y.; Li, G.; Zhang, Z.; Liang, J.; Mao, L.; Li, Y. Effects of reformed exhaust gas recirculation on the HC and CO emissions of a spark-ignition engine fueled with LNG. *Int. J. Hydrog. Energy* **2018**, *45*, 21070–21078. [CrossRef]
16. Catapan, R.C.; Cancino, L.R.; Oliveira, A.A.M.; Schwarz, C.; Nitschke, H.; Frank, T. Potential for onboard hydrogen production in a direct injection ethanol fueled spark ignition engine with EGR. *Fuel* **2018**, *234*, 441–446. [CrossRef]
17. Park, J.; Choi, J. A numerical investigation of lean operation characteristics of spark ignition gas engine fueled with biogas and added hydrogen under various boost pressures. *Appl. Therm. Eng.* **2017**, *117*, 225–234. [CrossRef]
18. Jung, S.Y.; Park, J. Numerical prediction of effects of CO_2 or H_2 content on combustion characteristics and generation efficiency of biogas-fueled engine generator. *Int. J. Hydrog. Energy* **2017**, *42*, 16991–16999. [CrossRef]
19. Ko, E.; Yoon, W.; Park, J. Fundamental characteristics of combustion under a spark ignition engine generator fueled by hydrogen-added biogas. *High Temp. High Press.* **2019**, *48*, 5–15. [CrossRef]
20. Yoon, W.; Ko, E.; Cho, H.; Park, J. A numerical investigation of hydrogen's effects on the performance of a heavy-duty natural-gas engine for a combined hydrogen, heat and power system. *High Temp. High Press.* **2019**, *48*, 25–36. [CrossRef]
21. Heywood, J.B. *Internal Combustion Engine Fundamentals*; McGraw Hill: New York, NY, USA, 1988.
22. McKay, M.C.; Beckman, R.J.; Conover, W.J. Comparison of three methods for selecting values of input variables in the analysis of output from a computer code. *Technometrics* **1979**, *21*, 239–245.
23. Park, J.; Song, S. Predicting the performance and NOx emissions of a turbocharged spark-ignition engine generator fueled with biogases and hydrogen addition under down-boosting condition. *Int. J. Hydrog. Energy* **2014**, *39*, 8510–8524. [CrossRef]
24. Park, J.; Lee, K.S.; Kim, M.S.; Jung, D. Numerical analysis of a dual-fueled CI (compression ignition) engine using Latin hypercube sampling and multi-objective Pareto optimization. *Energy* **2014**, *70*, 278–287. [CrossRef]